Composite Structures 273 (2021) 114278

Contents lists available at ScienceDirect

Composite Structures

journal homepage: www.elsevier.com/locate/compstruct

Buckling of cracked FG plate resting on elastic foundation considering the effect of delamination phenomenon

Do Van Thom [a,*], Ashraf M. Zenkour [b], Duc Hong Doan [c]

[a] Faculty of Mechanical Engineering, Le Quy Don Technical University, Hanoi City, Viet Nam
[b] Department of Mathematics, Faculty of Science, King Abdulaziz University, P.O. Box: 80203, Jeddah 21589, Saudi Arabia
[c] School of Transportation Engineering, Hanoi University of Science and Technology, Hanoi, Viet Nam

ARTICLE INFO

Keywords:
Delamination
Phase-field
Buckling
Crack
High-order shear
Functionally graded material

ABSTRACT

The buckling analysis of cracked functionally graded material (FGM) plates resting on an elastic foundation taking into account the effect of the delamination of the elastic foundation is presented in this paper. The plate kinematics are based on the high-order shear deformation theory, the buckling of this cracked plate is computed by mixing the phase-field theory and finite element method (FEM), and material properties are assumed to vary through the thickness direction by a power-law distribution. The cracked FGM plate rests on the two-parameter elastic foundation, in which, the delamination areas are rectangular and circular. The accuracy of the present approach is proved by the comparison with published results. This paper also studies the effect of some parameters on the mechanic buckling behavior of the plate. The numerical results reveal that the delamination area and the crack length have a strong effect on the buckling loads as well as the buckling mode shapes of this plate.

1. Introduction

Functionally graded material (FGM) is a new smart composite material, in which, the properties vary smoothly and continuously from one surface to one [13,15,21,36–40] or more surfaces [14]. The FGMs have many advantages in comparison with conventional layered composite materials such as reducing the stress concentration, thermal stresses, residual stresses, and so on. These are reasons for the wide application in engineering as thermal barrier coatings, biomedical materials, and piezoelectric devices. The FGM plate is a kind of structure and, it is very common in practice, for many working conditions, the plate can be appeared the defects (e.g., cracks), and then the mechanical behavior including the buckling of this plate has much change. Besides, many structures in practice can be modeled as a plate resting on an elastic foundation, for example, plates supported by the ground, water, and several types of liquid. The buckling behavior of the plate will change with the presence of a foundation. So that the research on the buckling problem is very interesting and helpful for designing and using this structure in practice.

There are many works published by scientists worldwide to understand the mechanical buckling behavior of FGM plates. Ma and Wang [1] studied the thermal bending and post-buckling of circular FGM plates based on first-order shear and third-order shear theories. The buckling of FGM plates subjected to thermal and mechanical loads was investigated by Ganapathi et al. [2] using a finite element solution. The analytical method and the classical plate theory were used in the work of Shariat and Eslami [3] to show out the thermal buckling response of imperfect FGM plates. Prakash et al. [4] presented a finite element solution for thermal post-buckling of FGM skew plates. Tran et al. [5] explored the stability of FGM plates in a thermal environment, in which, the study used isogeometric analysis and higher-order shear deformation theory. José et al. [6] proposed a finite element model for buckling and nonlinear static of FGM plates using Reddy's theory. Yang et al. [7] used first-order shear theory to research the buckling behavior of FGM plates resting on the two-parameter foundation. Thai and Kim [8] studied the buckling of FGM plates supported by the Pasternak foundation by an analytical method. Shariyat and Asemi [9] explored the shear buckling of FGM plates resting on the Winkler foundation. Yahoobi and Fereidoon [10] used Navier's solution for mechanical and thermal buckling of FGM plates which are resting on an elastic foundation. Duc and his co-workers [11] presented an analytical solution for nonlinear post-buckling of imperfect eccentrically stiffened FGM plates resting on the Pasternak elastic foundation. Zenkour and Radwan [41] investigated the response of

* Corresponding author.
E-mail address: thom.dovan@lqdtu.edu.vn (D. Van Thom).

https://doi.org/10.1016/j.compstruct.2021.114278
Received 3 May 2021; Revised 6 June 2021; Accepted 11 June 2021
Available online 15 June 2021

simply supported nanoplates resting on the elastic foundation using an analytical solution. Recently, the mechanical responses of structures taking into account the influence of elastic and non-elastic foundations have also been investigated in works [43–45].

To deal with crack problems, the meshfree method [12], FEM, the extended finite element method (XFEM) [16–19], the IGA, and the phase-field model [13,16–19,29–35] are used very commonly. However, the phase-field approach is more effective in difficult static and dynamic fracture problems. Readers can see in detail the advantages of the phase-field model in [23–25] and references therein. In this paper, we employ the phase-field model derived by Bourdin et al. [26,27] based on Griffith's theory [28] to give governing equations for buckling of FGM plates resting on a two-parameter elastic foundation. The buckling behavior of FGM plates takes into account the effect of the delamination between the plate and the foundation, as well as the crack to show out useful and interesting phenomenon, which is never done before.

The rest of this paper is presented as follows. Section 2 presents formulations of FEM and phase-field model for buckling analysis of cracked FGM plates supported by an elastic foundation. Numerical results of cracked FGM plates resting on the two-parameter elastic foundation are computed and discussed in Section 3. Some conclusions are given in Section 4.

2. Theoretical formulations

Consider a cracked FGM plate resting on the elastic foundation and having a delamination region from the elastic foundation as shown in Fig. 1. There are many computational theories for calculating plate and shell structures including classical and higher-order shear deformation theories, each one has certain advantages. Although the classical plate theory is simple to deal with, however, it does not take into account shear deformation, so this theory is only suitable for thin plates. The first-order shear deformation theory, although including shear strain, however, it requires the use of a shear correction factor and does not satisfy the condition of zero shear stress boundary at the plate surfaces. Therefore, the theory of high-order shear deformation theories, although complicated in calculations, satisfy the boundary condition of zero shear stress at the plate surfaces, and they do not need any shear correction factors, but still describes the mechanical response correctly of structures. As a result, due to this advantage, this work uses the third-order shear deformation theory [21] to solve the proposed problems. Using the third-order shear deformation theory, the displacements at a point (x,y,z) in the plate from mid-plane are written as [21]:

$$\begin{aligned} u(x,y,z) &= u_0(x,y) + \tfrac{5}{4}\left(z - \tfrac{4}{3h^2}z^3\right)\beta_x(x,y) + \left(\tfrac{1}{4}z - \tfrac{5}{3h^2}z^3\right)w_{0,x} \\ v(x,y,z) &= v_0(x,y) + \tfrac{5}{4}\left(z - \tfrac{4}{3h^2}z^3\right)\beta_y(x,y) + \left(\tfrac{1}{4}z - \tfrac{5}{3h^2}z^3\right)w_{0,y} \\ w(x,y,z) &= w_0(x,y) \end{aligned} \tag{1}$$

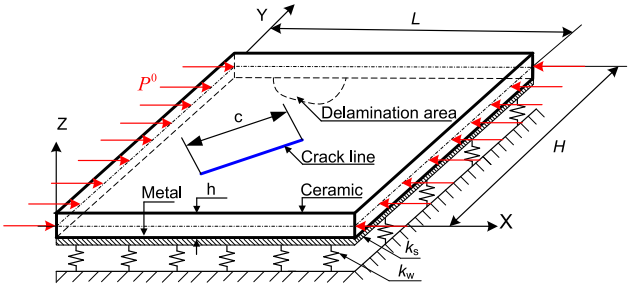

Fig. 1. Schematic geometry of a cracked FGM plate resting on an elastic foundation with the appearance of delamination between the foundation and the plate.

where h is the thickness; u_0, v_0, w_0 are the mid-plane displacements in the x-, y- and z-axes; β_x, β_y are the transverse normal rotations in the xz- and yz-planes.

$$\{\varepsilon\} = \begin{Bmatrix} \varepsilon_x = u_{0,x} + z\tfrac{1}{4}(5\beta_{x,x} + w_{,xx}) + z^3\left(\tfrac{-5}{3h^2}\right)(\beta_{x,x} + w_{,xx}) \\ \varepsilon_y = v_{0,y} + z\tfrac{1}{4}(5\beta_{y,y} + w_{,yy}) + z^3\left(\tfrac{-5}{3h^2}\right)(\beta_{y,y} + w_{,yy}) \\ \gamma_{xy} = u_{0,y} + v_{0,x} + z\tfrac{1}{4}(5\beta_{x,y} + 2w_{,xy} + 5\beta_{y,x}) + z^3\left(\tfrac{-5}{3h^2}\right)(\beta_{x,y} + 2w_{,xy} + \beta_{y,x}) \\ \gamma_{xz} = \tfrac{5}{4}(\beta_x + w_{,x}) + z^2\left(\tfrac{-5}{h^2}\right)(\beta_x + w_{,x}) \\ \gamma_{yz} = \tfrac{5}{4}(\beta_y + w_{,y}) + z^2\left(\tfrac{-5}{h^2}\right)(\beta_y + w_{,y}) \end{Bmatrix} \tag{2}$$

where the comma denotes the derivative of the variable following it.

The strains can be expressed as follow:

$$\varepsilon = \begin{Bmatrix} \varepsilon_0 \\ 0 \end{Bmatrix} + z\begin{Bmatrix} \kappa_1 \\ 0 \end{Bmatrix} + z^3\begin{Bmatrix} \kappa_3 \\ 0 \end{Bmatrix} + \begin{Bmatrix} 0 \\ \gamma_0 \end{Bmatrix} + z^2\begin{Bmatrix} 0 \\ \gamma_2 \end{Bmatrix} \tag{3}$$

where the mid-plane strain, the bending strain, and the shear strain in Eq. (3) are given as:

$$\varepsilon_0 = \begin{Bmatrix} u_{0,x} \\ v_{0,y} \\ u_{0,y} + v_{0,x} \end{Bmatrix};$$

$$\kappa_1 = \begin{Bmatrix} \tfrac{1}{4}(5\beta_{x,x} + w_{,xx}) \\ \tfrac{1}{4}(5\beta_{y,y} + w_{,yy}) \\ \tfrac{1}{4}(5\beta_{x,y} + 2w_{,xy} + 5\beta_{y,x}) \end{Bmatrix}; \kappa_3 = \begin{Bmatrix} \left(\tfrac{-5}{3h^2}\right)(\beta_{x,x} + w_{,xx}) \\ \left(\tfrac{-5}{3h^2}\right)(\beta_{y,y} + w_{,yy}) \\ \left(\tfrac{-5}{3h^2}\right)(\beta_{x,y} + 2w_{,xy} + \beta_{y,x}) \end{Bmatrix};$$

$$\gamma_1 = \begin{Bmatrix} \tfrac{5}{4}(\beta_x + w_{,x}) \\ \tfrac{5}{4}(\beta_y + w_{,y}) \end{Bmatrix}; \gamma_2 = \begin{Bmatrix} \left(\tfrac{-5}{h^2}\right)(\beta_x + w_{,x}) \\ \left(\tfrac{-5}{h^2}\right)(\beta_y + w_{,y}) \end{Bmatrix} \tag{4}$$

The internal forces can be obtained by operating the integral technique through the thickness as

$$\begin{Bmatrix} N \\ M \\ \bar{M} \\ Q \\ \bar{Q} \end{Bmatrix} = \begin{bmatrix} A & B & E & 0 & 0 \\ B & D & F & 0 & 0 \\ E & F & H & 0 & 0 \\ 0 & 0 & 0 & \bar{A} & \bar{B} \\ 0 & 0 & 0 & \bar{B} & \bar{D} \end{bmatrix} \begin{Bmatrix} \varepsilon_0 \\ \kappa_1 \\ \kappa_3 \\ \gamma_0 \\ \gamma_2 \end{Bmatrix} \tag{5}$$

with the material constant matrices are defined as follows:

$$\mathrm{A} = \begin{bmatrix} A_{11} & A_{12} & 0 \\ A_{12} & A_{22} & 0 \\ 0 & 0 & A_{66} \end{bmatrix}; \mathrm{B} = \begin{bmatrix} B_{11} & B_{12} & 0 \\ B_{12} & B_{22} & 0 \\ 0 & 0 & B_{66} \end{bmatrix}; \mathrm{D} = \begin{bmatrix} D_{11} & D_{12} & 0 \\ D_{12} & D_{22} & 0 \\ 0 & 0 & D_{66} \end{bmatrix} \tag{6}$$

$$\mathrm{E} = \begin{bmatrix} E_{11} & E_{12} & 0 \\ E_{12} & E_{22} & 0 \\ 0 & 0 & E_{66} \end{bmatrix}; \mathrm{F} = \begin{bmatrix} F_{11} & F_{12} & 0 \\ F_{12} & F_{22} & 0 \\ 0 & 0 & F_{66} \end{bmatrix}; \mathrm{H} = \begin{bmatrix} H_{11} & H_{12} & 0 \\ H_{12} & H_{22} & 0 \\ 0 & 0 & H_{66} \end{bmatrix} \tag{7}$$

$$\bar{A} = \begin{bmatrix} \bar{A}_{44} & 0 \\ 0 & \bar{A}_{55} \end{bmatrix}; \bar{B} = \begin{bmatrix} \bar{B}_{44} & 0 \\ 0 & \bar{B}_{55} \end{bmatrix}; \bar{D} = \begin{bmatrix} \bar{D}_{44} & 0 \\ 0 & \bar{D}_{55} \end{bmatrix} \tag{8}$$

in which the components in the expressions (6)-(8) are calculated as follows:

$$\{A_{ij}, B_{ij}, D_{ij}, E_{ij}, F_{ij}, H_{ij}\} = \int_{-h/2}^{h/2} J_{ij}\{1, z, z^2, z^3, z^4, z^6\}dz; \; i,j = 1,2,6 \tag{9}$$

$$\left\{\bar{A}_{ij}, \bar{B}_{ij}, \bar{D}_{ij}\right\} = \int_{-h/2}^{h/2} J_{ii}\{1, z^2, z^4\}dz; \; i = 4,5 \tag{10}$$

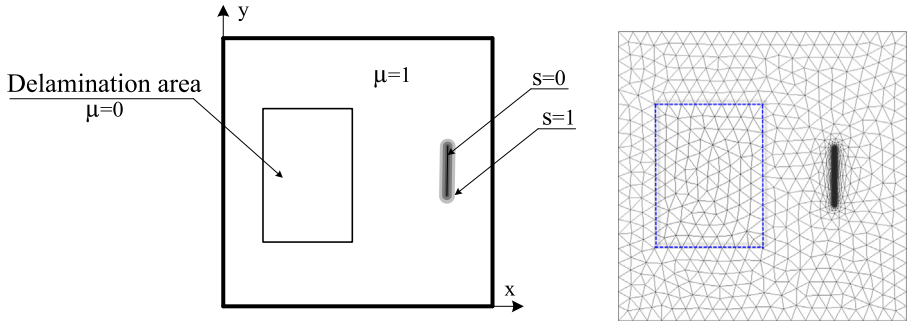

Fig. 2. A cracked FGM plate resting on an elastic foundation with the values of $\mu$and s.

with

$$J_{11} = J_{22} = \frac{E(z)}{1-\nu^2(z)};\ J_{12} = \nu(z).J_{22};\ J_{44} = J_{55} = J_{66} = \frac{E(z)}{2(1+\nu(z))} \tag{11}$$

with $E(z)$ and $\nu(z)$ are Young's modulus and Poisson's ratio, and they vary through the thickness by a power-law distribution defined for FGM plates. In this paper, we assume that an FGM plate made of a mixture of metal and ceramic, the material properties vary only along with the z-axis (Fig. 1), the top and bottom surfaces are fully ceramic and metallic. The xy-surface is the mid-surface of the plate, and the positive z-axis is upward from the mid-surface. The Young's modulus $E(z)$ and the Poisson's ratio $\nu(z)$ are the functions of z by a power-law distribution [22]

$$\left\{\begin{matrix} E(z) \\ \nu(z) \end{matrix}\right\} = \left\{\begin{matrix} E_m \\ \nu_m \end{matrix}\right\} + \left\{\begin{matrix} E_c - E_m \\ \nu_c - \nu_m \end{matrix}\right\}\left(\frac{h+2z}{2h}\right)^n \tag{12}$$

where n is the gradient index, z is the thickness coordinate variable ($-h/2 \leqslant z \leqslant h/2$), subscripts m, and c represent the metal and ceramic constituents, respectively.

For the buckling analysis of plate resting on the two-parameter foundation, the potential energy of FGM plate under in-plane compression force P^0 can be written as follows [13]:

$$\begin{aligned}
\Pi(\zeta,s) = {} & \tfrac{1}{2}\int_\Omega s^2 \left\{\begin{matrix} \varepsilon_0^T A\varepsilon_0 + \varepsilon_0^T B\kappa_1 + \varepsilon_0^T E\kappa_3 \\ +\kappa_1^T B\varepsilon_0 + \kappa_1^T D\kappa_1 + \kappa_1^T F\kappa_3 \\ +\kappa_3^T E\varepsilon_0 + \kappa_3^T F\kappa_1 + \kappa_3^T H\kappa_3 \\ +\gamma_0^T \breve{A}\gamma_0 + \gamma_0^T \breve{B}\gamma_2 + \gamma_2^T \breve{B}\gamma_0 + \gamma_2^T \breve{D}\gamma_2 \end{matrix}\right\} d\Omega + \\
& + \tfrac{1}{2}\int_\Omega s^2 \left\{\mu\left\{k_w w^2 + k_s\left(w_x^T w_x + w_y^T w_y\right)\right\}\right\} d\Omega \\
& + \tfrac{1}{2}\int_\Omega s^2 \left\{\begin{matrix} w_x \\ w_y \end{matrix}\right\}^T \sigma^{-0}\{w_x, w_y\} h dA + \tfrac{1}{2}\int_\Omega s^2 \left\{\begin{matrix} \beta_{x,x} \\ \beta_{x,y} \end{matrix}\right\}^T \sigma^{-0}\{\beta_{x,x}, \beta_{x,y}\} \tfrac{h^3}{12} d\Omega \\
& + \tfrac{1}{2}\int_\Omega s^2 \left\{\begin{matrix} \beta_{y,x} \\ \beta_{y,y} \end{matrix}\right\}^T \sigma^{-0}\{\beta_{y,x}, \beta_{y,y}\} \tfrac{h^3}{12} d\Omega + \int_\Omega G_C h\left[\tfrac{(1-s)^2}{4l} + l|\nabla s|^2\right] d\Omega \\
= {} & \int_\Omega \left\{\Psi(\zeta,s) + G_C\left[\tfrac{(1-s)^2}{4l} + l|\nabla s|^2\right] h\right\} d\Omega
\end{aligned} \tag{13}$$

where k_w and k_s are parameters of the elastic foundation, $\zeta = \{u_0, v_0, w_0, \beta_x, \beta_y\}$ is the vector of the degree of freedom, the matrix σ^{-0} is the pre-buckling stress subjected to the in-plane force:

$$\sigma^{-0} = \begin{bmatrix} \sigma_x^0 & 0 \\ 0 & \sigma_y^0 \end{bmatrix};\ \sigma_x^0 = \sigma_y^0 = \frac{P^0}{h} \tag{14}$$

and s is the phase-field variable as discussed in Section 1. In this paper, the phase-field approach is use, which was presented in detail by Bourdin et al. [26,27], the crack is modeled by a narrow region and controlled by the phase-field variable s which gets value from 0 (total broken) to 1 (unbroken). The fascinating point of this phase-field theory is that a discontinuous domain at the crack changes into a continuous domain through a transformation of variable s (Fig. 2). Because the crack becomes a continuous domain, it is easy to mesh the element at this position and interpolate the degrees of freedom of the plate as well as the phase-field variable values similar to the region without cracks, therefore, this makes the calculation simpler. Calculation theory for structures with cracks using phase-field variables presents a lot of advantages, making it easy to deal with because the discontinuity becomes a continuous domain, and especially shows a clear advantage when solving for plate problems with multiple cracks [18], and cracks with complex shapes [42], which is very difficult to solve with other methods. However, when a crack appears, the energy of the plate is reduced by the release of energy at the crack, which is shown in the component containing G_c in Equation (13), and the value of s^2 is multiplied by the rest of the energy expressions (13).

Also in the above expression, l is the length scale parameter, which controls the width of a region of the material where $s = 1$ and $s = 0$, and G_c is the critical energy release rate adopts Griffith's theory.

On the other hand, when taking into account the effect of the elastic foundation, the energy of the plate will be added by the energy of the foundation, which is proportional to the parameters k_w and k_s. It is noted that μ is parameter added in Eq. (13) to control the energy of the elastic foundation, which is attached to the FGM plate. It is assumed that this parameter gets two values, $\mu = 1$ if the elastic foundation is taken into account and $\mu = 0$ if the delamination between the plate and foundation appears (Fig. 2). In other words, the energy of the elastic foundation will be not added into the whole energy of the system at the delamination area.

Now, the plate is divided into the elements with n nodes, each node contains five degrees of freedom (DOF) $\zeta_i = \{u_{0i}, v_{0i}, w_{0i}, \beta_{xi}, \beta_{yi}\}$ and one DOF for phase-field variable s. Then, displacements and phase-field variable s at any points within one element are interpolated through interpolation functions as follows:

$$\zeta = \sum_{i=1}^{n} N_i\zeta_i = N\zeta_e;\ s = \sum_{i=1}^{n} N_i s_i = \hat{N}_s s_e \tag{15}$$

Representing deformation components according to node displacements, one gets:

$$\begin{aligned}
& \varepsilon_0 = B_0\zeta_e; \kappa_1 = B_1\zeta_e;\ \kappa_3 = B_3\zeta_e; \gamma_0 = B_{0\gamma}\zeta_e; \\
& \gamma_2 = B_{2\gamma}\zeta_e; w_0 = B_4\zeta_e;\ \frac{\partial w}{\partial x} = B_5\zeta_e;\ \frac{\partial w}{\partial y} = B_6\zeta_e
\end{aligned} \tag{16}$$

Table 1
Material properties of metal and ceramic.

Material	Properties		
	E (GPa)	ν	α ($1/^0$C)
Aluminum (Al)	70	0.3	23.10^{-6}
Alumina (Al_2O_3)	380	0.3	$7.4.10^{-6}$
Zirconia (ZrO_2)	151	0.3	10.10^{-6}

Table 2
Comparison of the normalized critical buckling coefficient $\bar{N}$ with $L/h = 20$.

$\bar{K}_w, \bar{K}_s$	$n = 0$			$n = 0.5$		
	Ref.	This work		Ref.	This work	
	[8]	Numbers of element		[8]	Numbers of element	
(0,0)	19.352	1250	19.426	12.566	1250	12.599
		1522	19.364		1522	12.407
		5462	19.274		5462	12.368
		6968	19.273		6968	12.363
(100,10)	22.112	1250	22.210	15.326	1250	15.401
		1522	22.160		1522	15.331
		5462	22.024		5462	15.114
		6968	22.022		6968	15.111
(10^3,10^2)	43.387	1250	43.403	33.049	1250	33.103
		1522	43.368		1522	32.912
		5462	42.976		5462	32.498
		6968	42.972		6968	32.495

Table 3
Comparison of the normalized critical buckling coefficient $\bar{N}$

$\bar{K}_w, \bar{K}_s$	L/h	Power-law index (n)					
		0		0.5		1	
		[8]	This work	[8]	This work	[8]	This work
(0, 0)	10	18.578	18.306	12.122	11.794	9.339	9.113
	20	19.352	19.273	12.566	12.363	9.667	9.536
	100	19.614	19.609	12.715	12.559	9.777	9.682
(100, 10)	10	21.337	21.025	14.882	14.513	12.098	11.832
	20	22.112	22.022	15.326	15.111	12.426	12.285
	100	22.373	22.368	15.475	15.318	12.536	12.441
(1000, 100)	10	40.647	39.388	31.460	30.236	27.431	26.427
	20	43.387	42.972	33.049	32.495	28.610	28.196
	100	44.388	44.368	33.620	33.366	29.033	28.875

$$\frac{\partial \beta_x}{\partial x} = B_7\zeta_e; \frac{\partial \beta_x}{\partial y} = B_8\zeta_e; \frac{\partial \beta_y}{\partial x} = B_9\zeta_e; \frac{\partial \beta_y}{\partial y} = B_{10}\zeta_e; \ \nabla s = B_{11}s_e \tag{17}$$

where:

$$\mathrm{B}_0 = \sum_{i=1}^{n}\begin{bmatrix} N_{i,x} & 0 & 0 & 0 & 0 \\ 0 & N_{i,y} & 0 & 0 & 0 \\ N_{i,y} & N_{i,x} & 0 & 0 & 0 \end{bmatrix}; \mathrm{B}_1 = \frac{1}{4}\sum_{i=1}^{n}\begin{bmatrix} 0 & 0 & N_{i,xx} & 5N_{i,x} & 0 \\ 0 & 0 & N_{i,yy} & 0 & 5N_{i,y} \\ 0 & 0 & 2N_{i,xy} & 5N_{i,y} & 5N_{i,x} \end{bmatrix} \tag{18}$$

$$\mathrm{B}_3 = \frac{-5}{3h^2}\sum_{i=1}^{n}\begin{bmatrix} 0 & 0 & N_{i,xx} & N_{i,x} & 0 \\ 0 & 0 & N_{i,yy} & 0 & N_{i,y} \\ 0 & 0 & 2N_{i,xy} & N_{i,y} & N_{i,x} \end{bmatrix}; \mathrm{B}_{0\gamma} = \frac{5}{4}\sum_{i=1}^{n}\begin{bmatrix} 0 & 0 & N_{i,x} & 1 & 0 \\ 0 & 0 & N_{i,y} & 0 & 1 \end{bmatrix}; \tag{19}$$

$$\mathrm{B}_{2\gamma} = \frac{-5}{h^2}\sum_{i=1}^{n}\begin{bmatrix} 0 & 0 & N_{i,x} & 1 & 0 \\ 0 & 0 & N_{i,y} & 0 & 1 \end{bmatrix}; \ \mathrm{B}_4 = \sum_{i=1}^{n}[0 \quad 0 \quad N_i \quad 0 \quad 0] \tag{20}$$

$$\mathrm{B}_5 = \sum_{i=1}^{n}[0 \quad 0 \quad N_{i,x} \quad 0 \quad 0]; \ \mathrm{B}_6 = \sum_{i=1}^{n}[0 \quad 0 \quad N_{i,y} \quad 0 \quad 0] \tag{21}$$

$$\mathrm{B}_7 = \sum_{i=1}^{n}[0 \quad 0 \quad 0 \quad N_{i,x} \quad 0]; \ \mathrm{B}_8 = \sum_{i=1}^{n}[0 \quad 0 \quad 0 \quad N_{i,y} \quad 0] \tag{22}$$

$$\mathrm{B}_9 = \sum_{i=1}^{n}[0 \quad 0 \quad 0 \quad 0 \quad N_{i,x}]; \ \mathrm{B}_{10} = \sum_{i=1}^{n}[0 \quad 0 \quad 0 \quad 0 \quad N_{i,y}]; \mathrm{B}_{11} = \sum_{i=1}^{n}\begin{bmatrix} N_{i,x} \\ N_{i,y} \end{bmatrix} \tag{23}$$

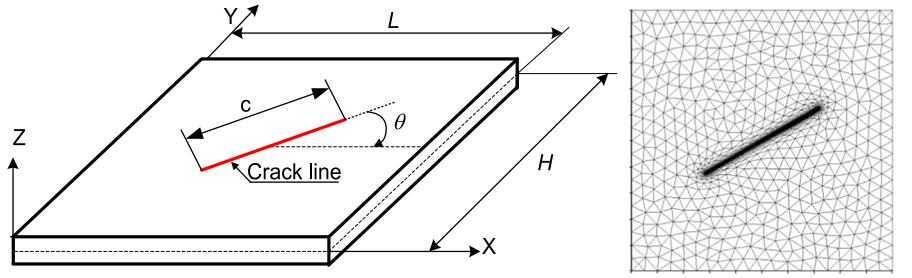

a. 3D view b. Mesh of the cracked plate

Fig. 3. The FGM plate with an inclined central crack.

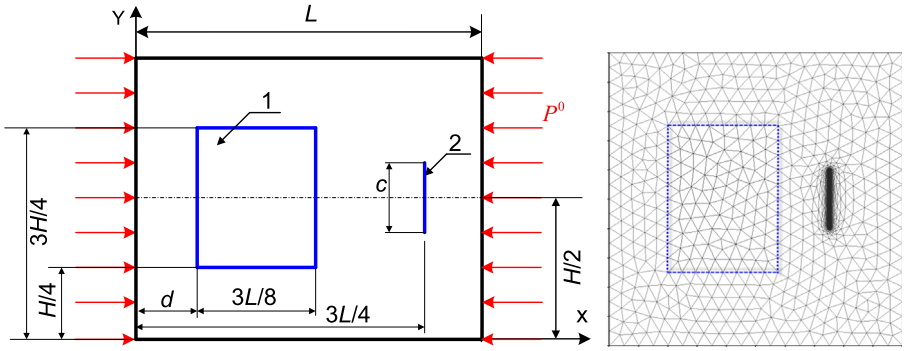

Fig. 4. The cracked FGM plate with a rectangular delamination area (1: the delamination area, 2: the crack).

The energy expression of the element will now be written in the following form:

$$\Pi_e(\zeta_e,s)=\tfrac{1}{2}\int_{\Omega_e}\hat{N}_s^T\hat{N}_s\zeta_e^T\left\{\begin{array}{c}B_0^TAB_0+B_0^TBB_1+B_0^TEB_3\\+B_1^TBB_0+B_1^TDB_1+B_1^TFB_3\\+B_3^TEB_0+B_3^TFB_1+B_3^THB_3\\+B_{0\gamma}^T\breve{A}B_{0\gamma}+B_{0\gamma}^T\breve{B}B_{2\gamma}+B_{2\gamma}^T\breve{B}B_{0\gamma}+B_{2\gamma}^T\breve{D}B_{2\gamma}\end{array}\right\}\zeta_e d\Omega+$$
$$+\tfrac{1}{2}\int_{\Omega_e}\hat{N}_s^T\hat{N}_s\zeta_e^T\left\{\mu\left\{k_wB_4^TB_4+k_s\left(B_5^TB_5+B_6^TB_6\right)\right\}\right\}\zeta_e d\Omega$$
$$+\tfrac{1}{2}\int_{\Omega_e}\hat{N}_s^T\hat{N}_s\zeta_e^T\left\{\begin{array}{c}B_5\\B_6\end{array}\right\}^T\sigma^{-0}\{B_5,\ B_6\}hdA+\tfrac{1}{2}\int_{\Omega_e}\hat{N}_s^T\hat{N}_s\zeta_e^T\left\{\begin{array}{c}B_7\\B_8\end{array}\right\}^T\sigma^{-0}\{B_7,\ B_8\}\tfrac{h^3}{12}d\Omega$$
$$+\tfrac{1}{2}\int_{\Omega_e}\hat{N}_s^T\hat{N}_s\zeta_e^T\left\{\begin{array}{c}B_9\\B_{10}\end{array}\right\}^T\sigma^{-0}\{B_9,\ B_{10}\}\tfrac{h^3}{12}d\Omega+\int_{\Omega_e}G_Ch\left[\frac{\left(1-\hat{N}_s\right)^2}{4l}+l\left|B_{11}^TB_{11}\right|^2\right]d\Omega$$
$$=\int_{\Omega_e}\left\{\Psi(\zeta_e,s)+hG_C\left[\frac{\left(1-\hat{N}_s\right)^2}{4l}+l\left|B_{11}^TB_{11}\right|^2\right]\right\}d\Omega \tag{24}$$

Table 4
Comparison of the CBTR of a fully simple support square Al/ZrO_2 plate

Method	Numbers of element	The volume fraction exponent (n)				
		0	0.5	1	2	5
XIGA [20]	–	8.894	6.114	5.412	5.012	4.771
This work	1250	8.956	6.123	5.498	5.180	4.806
	1522	8.882	6.119	5.418	5.164	4.773
	5462	8.716	6.039	5.401	5.049	4.746
	6968	8.712	6.035	5.400	5.047	4.742

Table 5
The critical buckling factor of cracked FGM depends on the crack length (c) and the volume fraction exponent (n) (uniaxial compression)

n	c/L	$\bar{K}_w,\bar{K}_s$				
		(0, 0)	(100, 0)	(100, 10)	(250, 25)	(1000, 100)
0	0.2	1.497	1.614	1.925	2.560	4.165
	0.3	1.390	1.503	1.799	2.363	4.018
	0.4	1.224	1.321	1.592	2.082	3.829
	0.5	1.053	1.136	1.390	1.848	3.644
0.5	0.2	1.164	1.280	1.591	2.210	3.630
	0.3	1.081	1.194	1.488	2.005	3.540
	0.4	0.952	1.049	1.315	1.779	3.420
	0.5	0.819	0.901	1.153	1.593	3.295
1	0.2	1.042	1.159	1.469	2.037	3.426
	0.3	0.968	1.081	1.374	1.863	3.356
	0.4	0.852	0.949	1.214	1.663	3.260
	0.5	0.733	0.815	1.065	1.497	3.158
2	0.2	0.956	1.072	1.383	1.911	3.277
	0.3	0.888	1.001	1.292	1.759	3.220
	0.4	0.782	0.878	1.141	1.579	3.142
	0.5	0.673	0.754	1.002	1.427	3.056
5	0.2	0.885	1.002	1.312	1.807	3.150
	0.3	0.822	0.935	1.225	1.672	3.104
	0.4	0.723	0.819	1.080	1.508	3.040
	0.5	0.622	0.703	0.951	1.369	2.968
10	0.2	0.830	0.946	1.256	1.725	3.047
	0.3	0.770	0.883	1.171	1.602	3.010
	0.4	0.678	0.773	1.033	1.452	2.956
	0.5	0.583	0.664	0.910	1.322	2.895

Minimizing the energy expression (24) according to displacements and phase-field variable we obtain the system of equations as follows:

$$\left\{\begin{array}{l}\delta\sum\Pi(\zeta_e,s_e,\delta\zeta)=0\\\delta\sum\Pi(\zeta_e,s_e,\delta s)=0\end{array}\right.\Longleftrightarrow\left\{\begin{array}{c}\left(\sum K^e+\lambda_{cr}\sum K_G^e\right)\zeta=0\\\sum\left\{\int_{\Omega_e}2\hat{N}_s^T\Psi(\zeta_e)\hat{N}_s d\Omega+\int_{\Omega_e}2G_Ch\left[-\frac{\left(1-\hat{N}_s^T\right)\hat{N}_s}{4l}+lB_{11}^TB_{11}\right]d\Omega\right\}=0\end{array}\right. \tag{25}$$

where λ_{cr} is the critical buckling load, and the matrices:

$$K^e=\int_{\Omega_e}\hat{N}_s^T\hat{N}_s\left\{\begin{array}{c}B_0^TAB_0+B_0^TBB_1+B_0^TEB_3\\+B_1^TBB_0+B_1^TDB_1+B_1^TFB_3\\+B_3^TEB_0+B_3^TFB_1+B_3^THB_3\\+B_{0\gamma}^T\breve{A}B_{0\gamma}+B_{0\gamma}^T\breve{B}B_{2\gamma}+B_{2\gamma}^T\breve{B}B_{0\gamma}+B_{2\gamma}^T\breve{D}B_{2\gamma}\end{array}\right\}d\Omega$$
$$+\int_{\Omega_e}\hat{N}_s^T\hat{N}_s\left\{\mu\left\{k_wB_4^TB_4+k_s\left(B_5^TB_5+B_6^TB_6\right)\right\}\right\}d\Omega \tag{26}$$

$$K_G^e=\int_{\Omega_e}\hat{N}_s^T\hat{N}_s\left\{\begin{array}{c}B_5\\B_6\end{array}\right\}^T\sigma^{-0}\{B_5,\ B_6\}hd\Omega+\tfrac{1}{2}\int_{\Omega_e}\hat{N}_s^T\hat{N}_s\left\{\begin{array}{c}B_7\\B_8\end{array}\right\}^T\sigma^{-0}\{B_7,\ B_8\}\tfrac{h^3}{12}d\Omega$$
$$+\tfrac{1}{2}\int_{\Omega_e}\hat{N}_s^T\hat{N}_s\left\{\begin{array}{c}B_9\\B_{10}\end{array}\right\}^T\sigma^{-0}\{B_9,\ B_{10}\}\tfrac{h^3}{12}d\Omega \tag{27}$$

Table 6
The critical buckling factor of cracked FGM depends on the crack length (c) and the volume fraction exponent (n) (biaxial compression)

n	c/L	$\bar{K}_w,\bar{K}_s$				
		(0, 0)	(100, 0)	(100, 10)	(250, 25)	(1000, 100)
0	0.2	0.753	0.811	0.966	1.281	2.720
	0.3	0.722	0.781	0.938	1.111	2.472
	0.4	0.677	0.737	0.897	1.049	2.365
	0.5	0.624	0.685	0.848	1.004	2.282
0.5	0.2	0.586	0.643	0.798	0.967	2.208
	0.3	0.561	0.620	0.777	0.938	2.145
	0.4	0.526	0.586	0.747	1.259	2.719
	0.5	0.485	0.546	0.709	1.096	2.470
1	0.2	0.524	0.582	0.737	1.036	2.362
	0.3	0.502	0.561	0.719	0.993	2.278
	0.4	0.471	0.531	0.691	0.958	2.203
	0.5	0.435	0.495	0.658	0.930	2.140
2	0.2	0.481	0.538	0.693	1.225	2.719
	0.3	0.461	0.520	0.677	1.072	2.468
	0.4	0.432	0.492	0.652	1.016	2.358
	0.5	0.399	0.459	0.622	0.898	2.273
5	0.2	0.445	0.503	0.658	0.976	2.198
	0.3	0.427	0.485	0.643	0.943	2.134
	0.4	0.400	0.460	0.620	0.917	2.718
	0.5	0.369	0.429	0.592	1.181	2.464
10	0.2	0.417	0.474	0.630	1.040	2.353
	0.3	0.400	0.459	0.615	0.989	2.267
	0.4	0.375	0.435	0.595	0.952	2.192
	0.5	0.346	0.406	0.569	0.922	2.128

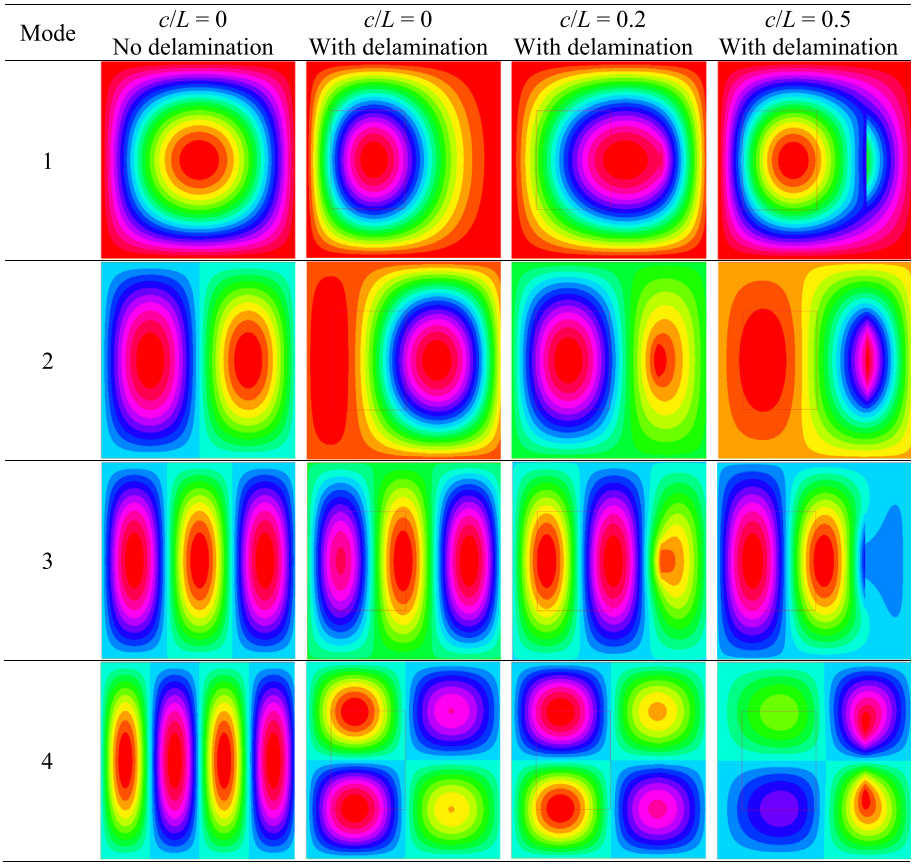

Fig. 5. The first four buckling mode shapes of FGM plate resting on an elastic foundation with $n = 0.5$ for different crack length (uniaxial load, $\bar{K}_w, \bar{K}_s = (250,25)$).

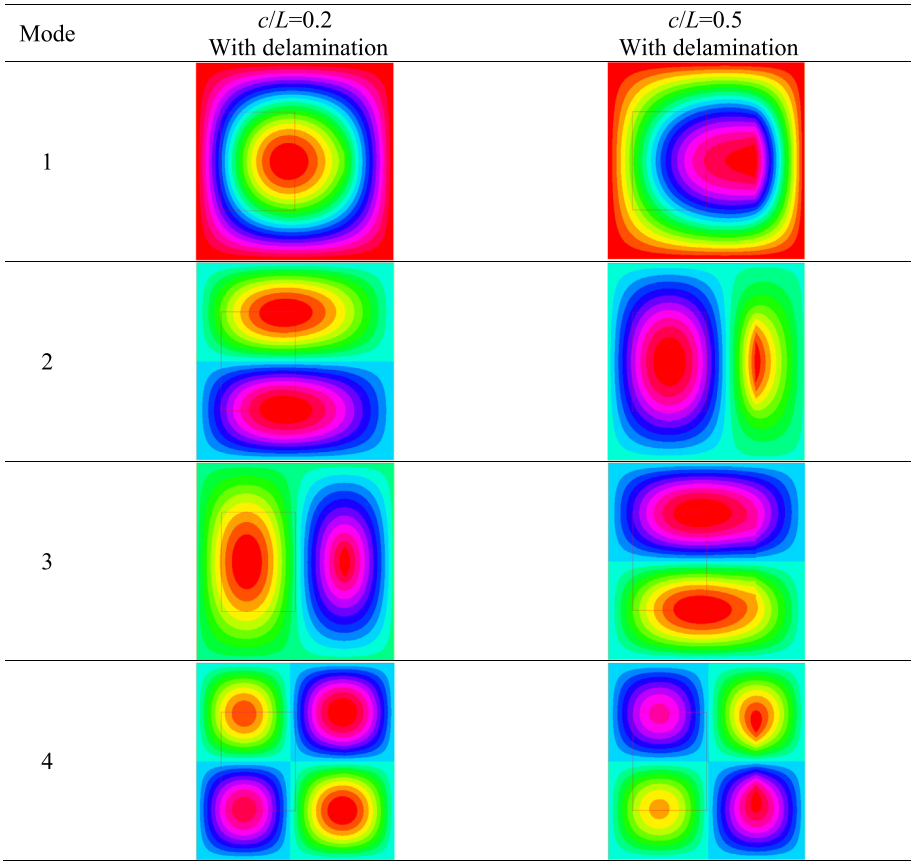

Fig. 6. The first four buckling mode shapes of FGM plate resting on an elastic foundation with $n = 0.5$ for different crack length (biaxial load, $\bar{K}_w, \bar{K}_s = (250,25)$).

According to [32], to form a crack, initial energy is required, and this energy has the following expression:

$$\Psi(s) = 10^3 \begin{cases} \frac{G_c}{4l} & x \leqslant \textit{crack length and } \frac{-l}{2} \leqslant y \leqslant \frac{l}{2} \\ 0 & \textit{else} \end{cases} \tag{28}$$

G_c is a specific quantity for a material, for fracture propagation problems, it changes continuously during the movement of the crack, but for the static crack problem, it is a constant to determine the crack shape, usually selected by 1. In general, G_c is a parameter depending on the material, which is determined through a material homogenization process according to the G_C^q value of the material components, G_c is employed only in Equation (28) to find the dimension of the crack. Accordingly, $\Psi(s)$ is selected as Equation (28) to consolidate $\Psi(s) > G_c$.

As a result, it is easy to find phase-field variable s from equation (25b), combining with equation (25a) it can be found critical loads and corresponding buckling mode shapes.

Note that herein variable μ appears in the element stiffness matrix expression that determines the effect of the elastic foundation at the region has the delamination between the plate and foundation; this parameter is set to be 0, in other regions it takes a value of 1 (Fig. 2).

Table 7
The critical buckling factor of cracked FGM depends on the crack length (c) and distance d (uniaxial load, $n = 0.5$)

L/d	c/L	$\bar{K}_w, \bar{K}_s$				
		(0, 0)	(100, 0)	(100, 10)	(250, 25)	(1000, 100)
8	0.2	1.164	1.280	1.591	2.210	3.630
	0.3	1.081	1.194	1.488	2.005	3.540
	0.4	0.952	1.049	1.315	1.779	3.420
	0.5	0.819	0.901	1.153	1.593	3.295
5	0.2	1.164	1.263	1.583	2.177	3.610
	0.3	1.081	1.179	1.473	1.959	3.483
	0.4	0.952	1.038	1.300	1.739	3.332
	0.5	0.819	0.894	1.139	1.558	3.191
16/5	0.2	1.164	1.247	1.573	2.103	3.486
	0.3	1.081	1.158	1.451	1.875	3.250
	0.4	0.952	1.018	1.270	1.649	3.005
	0.5	0.819	0.876	1.108	1.468	2.799

3. Numerical results

3.1. Accuracy study

In this section, two cases of the comparisons to illustrate the accuracy of this method in buckling analysis are presented. Firstly, an FGM (Al/Al_2O_3) plate resting on the two-parameter foundation is considered. The plate is set up to be $L/H = 1$, thickness h varies from $L/10$ to $L/100$, the material properties are given in Table 1, and is subjected to uniaxial compression. The numerical results of the normalized critical buckling coefficient obtained by the present method for different numbers of the element are compared with the analytical method [8] as listed in Table 2 ($L/h = 20$), and it can be observed that the 6968-element mesh can ensure the necessary accuracy and convergence rate of the calculation program. Note that the numerical results obtained in Table 3 used this mesh.

Compared with the reference method [8], it can see that a good agreement is obtained. In this example, the parameters are normalized by [8]

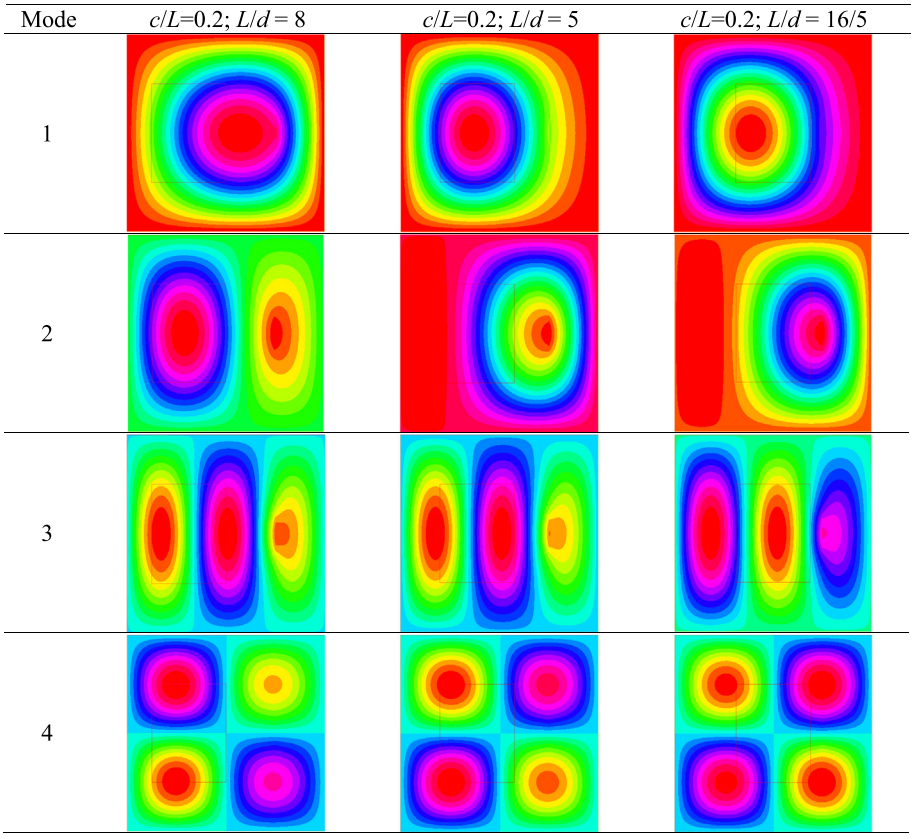

Fig. 7. The first four buckling mode shapes of FGM plate resting on an elastic foundation with $n = 0.5$ for different distance d (uniaxial load, $c/L = 0.2$, $\bar{K}_w, \bar{K}_s =$ (250,25)).

$$\bar{N} = \lambda_{cr}\frac{L^2}{E_m h^3};\ \bar{K}_w = \frac{k_w L^4}{D_m};\ \bar{K}_s = \frac{k_s L^2}{D_m};\ D_m = \frac{E_m h^3}{12(1-\nu^2)} \tag{29}$$

The accuracy of this method is further studied by examining a fully simple supported square FGM (Al/ZrO_2) plate. The plate geometry is set to be $L = H = 1$ m, $h = 0.01$ m, the plate has a crack which is at the center of this plate as shown in Fig. 3, the material properties are listed in Table 1. The critical buckling temperature rise (CBTR) [20] for cracked FGM plate is investigated ($c/L = 0.6$,) and compared with those of this work as shown in Table 4. The accuracy of this method is confirmed as a good agreement between the calculated results and the extended isogeometric analysis (XIGA) method is found. The numerical results are performed with a mesh with increasing numbers of elements, and when the mesh has 6968 elements, the convergence rate reaches the required precision. Therefore, the following computed data are operated with this mesh.

3.2. Numerical studies

In this section, numerical results to find out the effect of the crack and the delamination phenomenon between the plate and the foundation on the buckling behavior of the cracked FGM (Al/ ZrO_2) plate is shown. This plate is square with $L/H = 1$, thickness $h = L/100$, and all edges are simply supported, in which, the crack length c can be changed, this plate is subjected to uniaxial compression in the x-axis

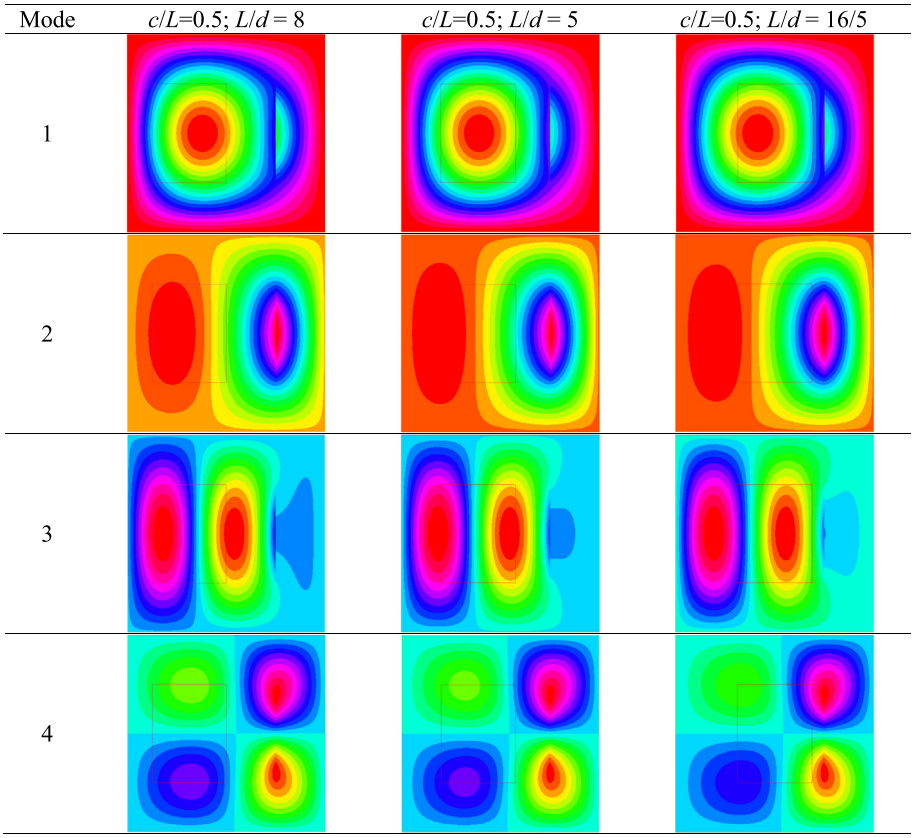

Fig. 8. The first four buckling mode shapes of FGM plate resting elastic foundation with $n = 0.5$ for different distance d (uniaxial load, $c/L = 0.5$, $\bar{K}_w, \bar{K}_s =$ (250,25)).

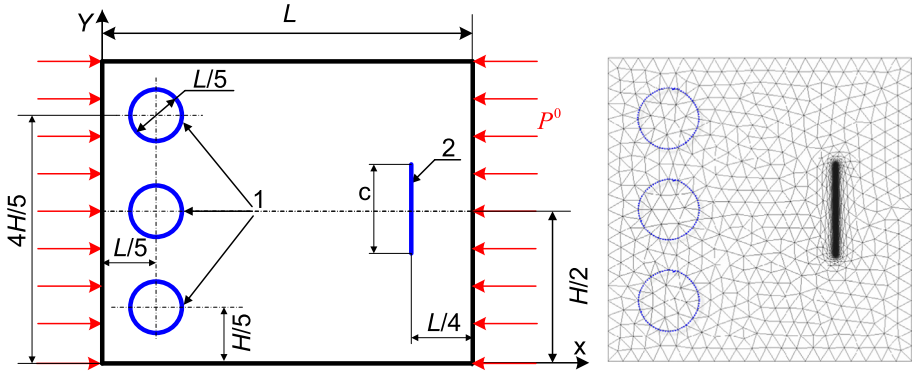

Fig. 9. The cracked FGM plate with three circle delamination areas (1: the delamination area, 2: the crack).

Table 8
The buckling critical load of cracked FGM depends on the crack length (c) and the volume fraction exponent (uniaxial load)

n	c/L	$\bar{K}_w, \bar{K}_s$				
		(0, 0)	(100, 0)	(100, 10)	(250, 25)	(1000, 100)
0	0.2	1.497	2.363	3.688	5.942	15.640
	0.3	1.390	2.036	3.405	5.669	15.561
	0.4	1.224	1.722	3.097	5.352	15.392
	0.5	1.053	1.472	2.838	5.077	15.137
0.5	0.2	1.164	1.903	3.204	5.449	14.304
	0.3	1.081	1.654	2.989	5.236	14.275
	0.4	0.952	1.406	2.751	4.979	14.227
	0.5	0.819	1.209	2.549	4.754	14.157
1	0.2	1.042	1.730	3.026	5.266	13.741
	0.3	0.968	1.510	2.835	5.077	13.725
	0.4	0.852	1.288	2.622	4.839	13.701
	0.5	0.733	1.110	2.440	4.632	13.666
2	0.2	0.956	1.606	2.362	5.136	13.315
	0.3	0.888	1.406	2.900	4.962	13.305
	0.4	0.782	1.203	2.725	4.739	13.290
	0.5	0.673	1.039	2.530	4.543	13.271
5	0.2	0.885	1.504	2.797	5.027	12.946
	0.3	0.822	1.320	2.635	4.867	12.939
	0.4	0.723	1.132	2.453	4.655	12.931
	0.5	0.622	0.980	2.298	4.469	12.919
10	0.2	0.830	1.424	2.715	4.941	12.644
	0.3	0.770	1.252	2.563	4.792	12.639
	0.4	0.678	1.076	2.393	4.588	12.633
	0.5	0.583	0.933	2.246	4.409	12.626

or biaxial compression. Two parameters of foundation and critical buckling load N' are normalized as in Eq.(29).

3.2.1. The cracked FGM plate resting on an elastic foundation with a rectangular delamination area (Fig. 4)

3.2.1.1. Effect of the crack length (c) and the volume fraction exponent index (n). In this subsection, the distance $d = L/8$ is selected. To get the influence of relative crack length c, material gradation on the buckling load of cracked FGM plate with a rectangular delamination area, the crack-length ratio c/L increases from 0.2 to 0.5 and the gradient index varies from 0 to 10. Tables 5 and 6 show the critical buckling factor computed for each ratio c/L and each gradient index n for both uniaxial and biaxial compressions. It can see that for both cases of compressive load, the buckling factor N' decreases with an increase in the crack length c, the same behavior for increasing gradient index n. These decreases can be explained that the energy release surface becomes larger, and the stiffness of plates decreases with an increase in the crack length c. The metallic volume fraction of the FGM plate increases when n increases, the stiffness decreases, and buckling factor N' decreases. The parameters of the foundation increase, the structure becomes stiffer, and the buckling load increases. It also finds the amplitude of buckling factor N' for the biaxial load is smaller than that for the uniaxial load.

Fig. 5 plots the first four buckling mode shapes of FGM plate under the uniaxial load with four cases, case 1: no crack ($c/L = 0$) and no delamination, case 2: no crack and with delamination areas, case 3: with crack $c/L = 0.2$, and with delamination area, case 4: with crack $c/L = 0.5$ and with delamination. Fig. 6 is shown for FGM plates under the biaxial load with delamination area in two cases of crack length $c/L = 0.2$ and 0.5. It can be seen in Figs. 5 and 6 for both cases that the crack length and the delamination phenomenon between the plate and the elastic foundation play an important effect on the value of buckling load as well as buckling mode shapes of FGM plates.

3.2.1.2. Effect of the location of delamination area. The effect of the location of the delamination area on buckling behavior is investigated. The FGM plate subjected to uniaxial load with $n = 0.5$ is taken. The distance d between the left edge and the delamination area (see Fig. 4) changes from $L/8$ to $5L/16$, it means that the delamination area moves from the left to the center of the plate, and the distance between the crack and the delamination area decreases. The numerical results listed in Table 7 show that the delamination area is nearer the plate center, the critical buckling load becomes smaller, this means that when the delamination area is closer to the crack as well as the center of the plate, the energy of the plate releases more, and therefore, the plate is softer.

It can see clearly that the buckling modes plotted in Figs. 7 and 8 are very interesting. The location of the delamination area has a strong effect on buckling modes in this study.

Table 9
The buckling critical load of cracked FGM depends on the crack length (c) and the location of the delamination area (uniaxial load, $n = 0.5$)

	c/L	$\bar{K}_w, \bar{K}_s$				
		(0, 0)	(100, 0)	(100, 10)	(250, 25)	(1000, 100)
Case 1	0.2	1.164	1.903	3.204	5.449	14.304
	0.3	1.081	1.654	2.989	5.236	14.275
	0.4	0.952	1.406	2.751	4.979	14.227
	0.5	0.819	1.209	2.549	4.754	14.157
Case 2	0.2	1.164	1.901	3.192	5.412	14.263
	0.3	1.081	1.653	2.971	5.187	14.220
	0.4	0.952	1.405	2.732	4.930	14.151
	0.5	0.819	1.207	2.531	4.709	14.056
Case 3	0.2	1.164	1.897	3.186	5.402	14.228
	0.3	1.081	1.638	2.938	5.142	14.177
	0.4	0.952	1.389	2.680	4.842	14.021
	0.5	0.819	1.191	2.462	4.575	13.885

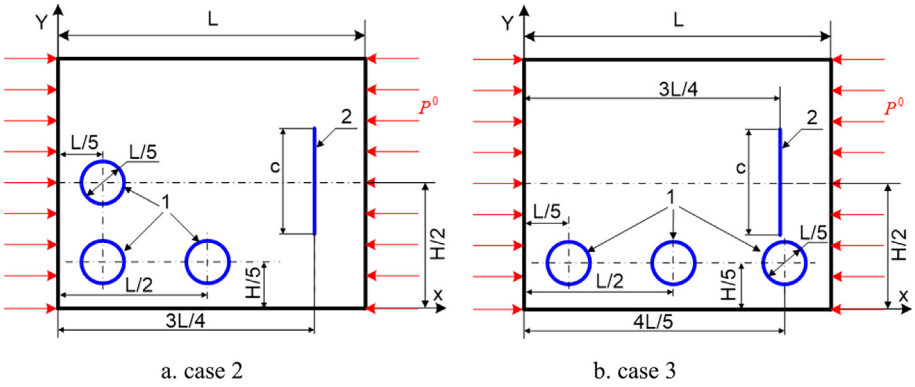

Fig. 10. Model geometry of two cracked FGM plates with three delamination areas (1: the delamination area, 2: the crack).

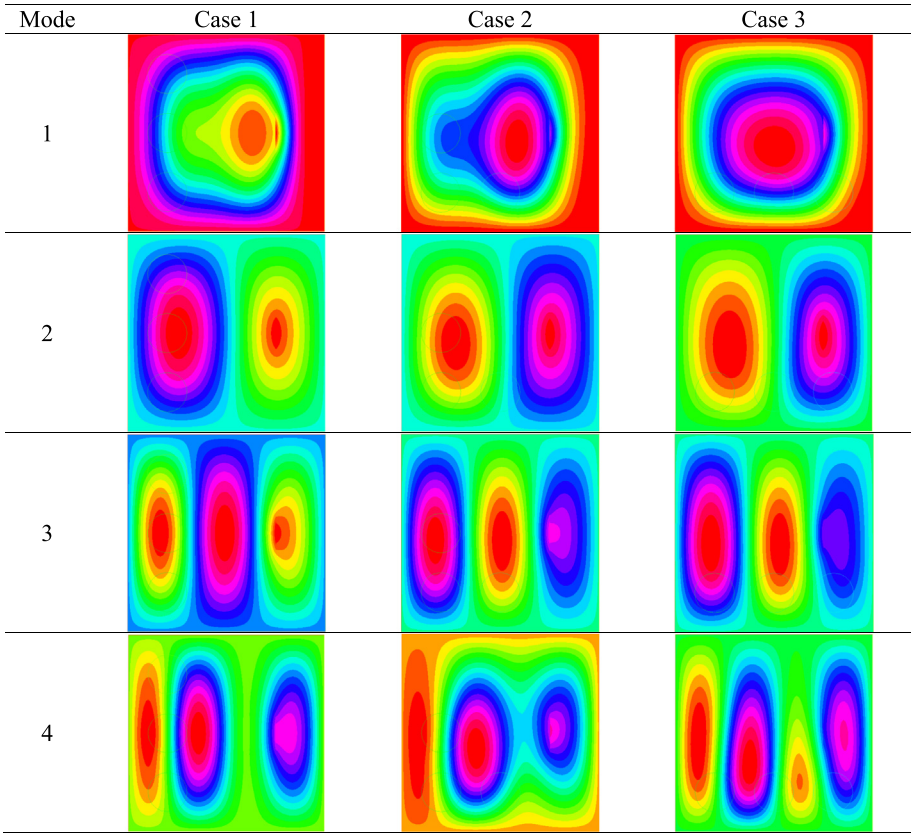

Fig. 11. The first four buckling mode shapes of FGM plate resting on an elastic foundation for three cases of delamination area ($n = 0.5$, $c/L = 0.2$, $\bar{K}_w, \bar{K}_s = (250,25)$).

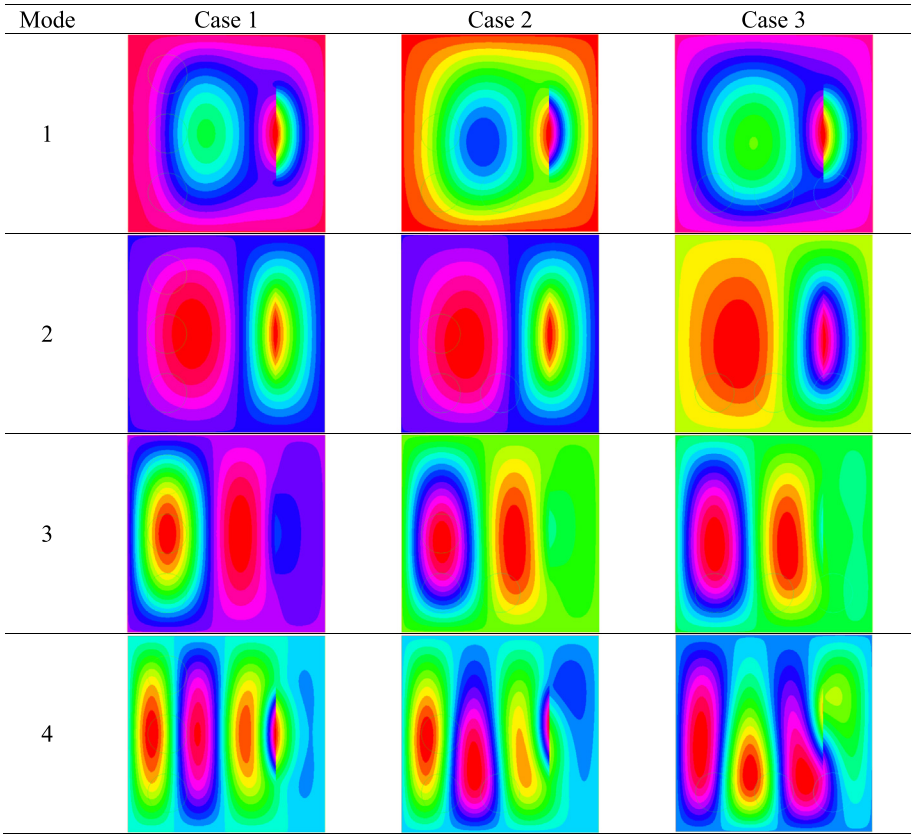

Fig. 12. The first four buckling mode shapes of FGM plate resting on an elastic foundation for three cases of delamination area ($n = 0.5$, $c/L = 0.5$, $\bar{K}_w, \bar{K}_s = (250,25)$).

3.2.2. The cracked FGM plate resting on an elastic foundation with three circle delamination areas (Fig. 9)

3.2.2.1. Effect of the crack length (c) and the volume fraction exponent index (n). In this subsection, the cracked FGM plate with three circle delamination areas is explored. Table 8 lists the buckling factor for various crack-length (c/L) and gradient indices, the parameters are set to be c/L = 0.2–0.5, n = 0–10, the plate is subjected to uniaxial load. It also can be observed that when the crack length and n increases, the critical buckling load decreases.

3.2.2.2. Effect of the location of the delamination area. Three cases of the location of the delamination area are analyzed, case 1: three circle delamination areas are shown in Fig. 9, case 2: three circle delamination areas are shown in Fig. 10a and case 3 is shown in Fig. 10b.

The computed results of the buckling factor are given in Table 9. We can see that the buckling load in the first case is higher than it in the second case, the buckling load in the third case is smaller than it in the second case. This means that the stiffness of the FGM plate in the third case is the smallest and in the first case is highest. This also shows that the closer the delamination area is to the crack, the softer the plate becomes. In addition, as the elastic foundation parameter increases, the energy of the plate increases, causing the overall stiffness of the plate to increase, so that the critical buckling load of the plate also increases. Besides, as the crack length c of the plate increases, the critical buckling load decreases due to the energy is released through the increase of the crack length.

The first four buckling mode shapes of these plates obtained by this method in three cases with two values of the crack-length c/L are plotted in Figs. 11 and 12. It is very interesting as it reveals a significant impact of the delamination areas on the buckling load as well as the buckling mode shapes.

4. Conclusions

In this paper, a new numerical research of the effect of the delamination phenomenon between the plate and the elastic foundation and the crack on buckling behaviors of cracked FGM plate resting on a two-parameter foundation is carried out. The formulations are based on the third-order shear theory and FEM, the crack is modeled by a parameter called phase-field variable. The effects of various parameters in two kinds of delamination area (rectangular and circle) on the buckling behavior are explored in detail. The present method is flexible and cannot be limited to solve other complex problems. From numerical results, some conclusions are figured out as follows:

- The combining of the delamination area and the crack has an important and interesting effect on buckling mode shapes as well as buckling load. For the considered cases, the closer the delamination area is to the crack, the more the hardness of the plate decreases, the plate becomes softer.
- For the FGM plate, the buckling load decreases with the increases of the volume fraction index. This as the increase of metallic volume when the gradient index increase will make the stiffness of the FGM plate softer.
- The increasing the crack length c leads to a decrease of buckling load, this due to the energy surface release increases. The crack length also has a strong effect on the buckling modes of cracked FGM plates.
- The buckling load is reduced as the relative parameters of the elastic foundation decrease.

5. Data availability

Data used to support the findings of this study are included in the article.

Declaration of Competing Interest

The authors declare that they have no known competing financial interests or personal relationships that could have appeared to influence the work reported in this paper.

Acknowledgments

Do Van Thom gratefully acknowledges the support of Vietnam National Foundation for Science and Technology Development (NAFOSTED) under grant number 107.02-2018.30.

References

[1] Ma LS, Wang TJ. Nonlinear bending and postbuckling of functionally graded circular plates under mechanical and thermal loadings. Int. J. Nonlinear Mech. 2003;40:3311–30.
[2] Ganapathi M, Prakash T, Sundararajan N. Influence of functionally graded material on buckling of skew plates under mechanical loads. ASCE J Eng Mech 2006;132:902–5.
[3] Shariat BA, Eslami MR. Buckling of thick functionally graded plates under mechanical and thermal loads. Compos Struct 2007;78:433–9.
[4] Prakash T, Singha MK, Ganapathi M. Thermal postbuckling analysis of FGM skew plates. Eng Struct 2008;30:22–32.
[5] Tran LV, Phung-Van P, Lee J, Wahab MA, Nguyen-Xuan H. Isogeometric analysis for nonlinear thermomechanical stability of functionally graded plates. Compos Struct 2016;140:655–67.
[6] Moita JS, Araújo AL, Correia VF, Mota CM, Soares JH. Buckling and Nonlinear Response of Functionally Graded Plates Under Thermo-Mechanical Loading. Compos Struct 2018. Available online 21 March 2018.
[7] Yang J, Liew K, Kitipornchai S. Second order statistics of the elastic buckling of functionally graded rectangular plates. Compos Sci Technol 2005;65:1165–75.
[8] Thai HT, Kim SE. Closed-form solution for buckling analysis of thick functionally graded plates on elastic foundation. Int J Mech Sci 2013;75:34–44.
[9] Shariyat M, Asemi K. Three-dimensional nonlinear elasticity-based 3D cubic B-spline finite element shear buckling analysis of rectangular orthotropic FGM plates surrounded by elastic foundations. Composite Part B 2014;56:934–47.
[10] Yaghoobi H, Fereidoon A. Mechanical and thermal buckling analysis of functionally graded plates resting on elastic foundations: An assessment of a simple refined nth-order shear deformation theory. Composite Part B 2014;56:54–64.
[11] Duc ND, Cong PH. Nonlinear postbuckling of an eccentrically stiffened thin FGM plate resting on elastic foundations in thermal environments. Thin-walled Structures 2014;75:103–12.
[12] Khosravifard A, Hematiyan MR, Bui TQ, Thom VD. Accurate and efficient analysis of stationary and propagating crack problems by meshless methods. Theor Appl Fract Mech 2017;87:21–34.
[13] Thom VD, Duc HD, Duc ND, Tinh QB. Phase-field thermal buckling analysis for cracked functionally graded composite plates considering neutral surface. Compos Struct 2017;182:524–48.
[14] Thom VD, Kien ND, Duc ND, Duc HD, Tinh QB. Analysis of bi-directional functionally graded plates by FEM and a new third-order shear deformation plate theory. Thin-Walled Struct 2017;119:687–99.
[15] Thom VD, Tinh QB, Yu TT, Dat PT, Chung TN. Role of material combination and new results of mechanical behavior for FG sandwich plates in thermal environment. J Comput Sci 2017;21:164–81.
[16] Duc HD, Tinh QB, Thom VD, Duc ND. A rate-dependent hybrid phase field model for dynamic crack propagation. J Appl Phys 2017;122(115102):1–4.
[17] Duc HD, Thom VD, Phuc MP, Duc ND. Validation simulation for free vibration and buckling of cracked Mindlin plates using phase-field method. Mech Adv Mater Struct 2018:1–10.
[18] Duc ND, Truong TD, Thom VD, Duc HD. On the Buckling Behavior of Multi-cracked FGM Plates. Procceeding of the International Conference on Advances in Computational Mechanics 2017, Lecture Notes in Mechanical Engineering: 29-45.
[19] Phuc MP, Thom VD, Duc HD, Duc ND. The stability of cracked rectangular plate with variable thickness using phasefield method. Thin-Walled Struct 2018;129:157–65.
[20] Yu TT, Tinh QB, Shuohui Y, Duc HD, Wu CT, Thom VD, et al. On the thermal buckling analysis of functionally graded plates with internal defects using extended isogeometric anlysis. Compos Struct 2016;136:684–95.
[21] Tinh QB, Thom VD, Lan HTT, Duc HD, Satoyuki T, Dat TP, et al. On the high temperature mechanical behaviors analysis of heated functionally graded plates using FEM and a new third-order shear deformation plate theory. Composite part B 2016;92:218–41.
[22] Reddy JN. Analysis of functionally graded plates. Int J Num Method Eng 2000;47:663–84.
[23] Miehe C, Hofacker M, Welschinger F. A phase field model for rate-independent crack propagation: robust algorithmic implementation based on operator splits. Comput Meth Appl. Mech Eng 2010;199:2766–78.
[24] Doan HD, Bui QT, Nguyen DD, Fushinobu K. Hybrid phase field simulation of dynamic crack propagation in functionally graded glass-filled epoxy. Compos Part B 2016;99:266–76.

[25] Michael JB, Clemens VV, Michael AS, Thomas JRH, Chad ML. A phase-field description of dynamic brittle fracture. Comput. Methods Appl. Mech. Engrg. 2012;217–220:77–95.
[26] Bourdin B, Francfort GA, Marigo JJ. Numerical experiments in revisited brittle fracture. J Mech Phys Solids 2000;48:797–826.
[27] Bourdin B, Francfort GA, Marigo JJ. The variableal approach to fracture. J Elast 2008;91:5–148.
[28] Francfort GA, Marigo JJ. Revisiting brittle fractures as an energy minimization problem. J Mech Phys Solids 1998;46:1319–42.
[29] Amor H, Marigo JJ, Maurini C. Regularized formulation of the variableal brittle fracture with unilateral contact: Numerical experiments. J Mech Phys Solids 2009;57:1209–29.
[30] Kuhn C, Muller R. A continuum phase field model for fracture. Eng Fract Mech 2010;77:3625–34.
[31] Miehe C, Hofacker M, Welschinger F. A phase field model for rate-independent crack propagation: robust algorithmic implementation based on operator splits. Comput Methods in Apl Mech Eng 2010;199:2765–78.
[32] Borden MJ, Verhoosel CV, Scott MA, Hughes TJR, Landis CM. A phase-field description of dynamic brittle fracture. Comput Methods Appl Mech Eng 2012;217–220:77–95.
[33] Gerasimov T, De Lorenzis L. A line search assisted monolithic approach for phase-field computing of brittle fracture. Comput Methods Appl Mech Eng 2016;312:276–303.
[34] Ambati M, Gerasimov T, De Lorenzis L. A review on phase-field models of brittle fracture and a new fast hybrid formulation. Comput Mech 2014;55:383–405.
[35] Nam VH, Duc HD, Nguyen MK, Thom VD, Hong TT. Phase-field buckling analysis of cracked stiffened functionally graded plates. Compos Struct 2019;217:50–9.
[36] Tran TT, Tran VK, Pham Q-H, Zenkour AM. Extended four-unknown higher-order shear deformation nonlocal theory for bending, buckling and free vibration of functionally graded porous nanoshell resting on elastic foundation. Compos Struct 2021;264(15):113737.
[37] Zenkour AM, Radwan AF. Bending and buckling analysis of FGM plates resting on elastic foundations in hygrothermal environment. Archiv Civil Mech Eng 2020;20:112. 23 pages.
[38] Daikh AA, Zenkour AM. Bending of functionally graded sandwich nanoplates resting on Pasternak foundation under different boundary conditions. J Appl Comput Mech 2020;6(SI):1245–59.
[39] Zenkour AM, Alghanmi RA. Static response of sandwich plates with FG core and piezoelectric faces under thermo-electro-mechanical loads and resting on elastic foundations. Thin-Walled Struct 2020;157:107025 (18 pages).
[40] Sobhy M, Zenkour AM. A comprehensive study on the size-dependent hygrothermal analysis of exponentially graded microplates on elastic foundations. Mech Adv Mater Struct 2020;27(10):816–30.
[41] Zenkour AM, Radwan AF. Nonlocal mixed variational formula for orthotropic nanoplates resting on elastic foundations. Eur Phys J Plus 2020;135:493 (19 pages).
[42] Doan DH, Do VT, Nguyen XN, Vinh PV, Trung NT. Multi-phase-field modelling of the elastic and buckling behaviour of laminates with ply cracks. Appl Math Model 2021;94:68–86.
[43] Saeed IT, Abdelbaki C, Abdelouahed T, Al-OstaaSalah MA, Al-Dulaijan SU, Al-Zahrania MM. Wave propagation analysis of a ceramic-metal functionally graded sandwich plate with different porosity distributions in a hygro-thermal environment. Compos Struct 2021;269:114030.
[44] Al-Furjan MSH, Ali H, Mostafa H, Lijun S, Abdelouahed T. On the vibrations of the imperfect sandwich higher-order disk with a lactic core using generalize differential quadrature method. Compos Struct 2021;257:113150.
[45] Refrafi S, Bousahla AA, Bouhadra A, Menasria A, Bourada F, Tounsi A, et al. Effects of hygro-thermo-mechanical conditions on the buckling of FG sandwich plates resting on elastic foundations. Comput Concr 2020;25(4):311–25.